ACS Chemical Neuroscience

Research Article

pubs.acs.org/chemneuro

Neuron Subpopulations with Different Elongation Rates and DCC Dynamics Exhibit Distinct Responses to Isolated Netrin-1 Treatment

Agata Blasiak, Gil U. Lee,*,† and Devrim Kilinc*,†

Bionanoscience Group, School of Chemistry and Chemical Biology, University College Dublin, Belfield, Dublin 4, Ireland

Supporting Information

ABSTRACT: Correct wiring of the nervous system requires guidance cues, diffusible or substrate-bound proteins that steer elongating axons to their target tissues. Netrin-1, the best characterized member of the Netrins family of guidance molecules, is known to induce axon turning and modulate axon elongation rate; however, the factors regulating the axonal response to Netrin-1 are not fully understood. Using microfluidics, we treated fluidically isolated axons of mouse primary cortical neurons with Netrin-1 and characterized axon elongation rates, as well as the membrane localization of deleted in colorectal cancer (DCC), a well-established receptor of Netrin-1. The capacity to stimulate and observe a large number of individual axons allowed us to conduct distribution analyses, through which we identified two distinct neuron subpopulations based on different elongation behavior and different DCC membrane dynamics. Netrin-1 reduced the elongation rates in both subpopulations, where the effect was more pronounced in the slow growing subpopulation. Both the source of Ca^{2+} influx and the basal cytosolic Ca^{2+} levels regulated the effect of Netrin-1, for example, Ca^{2+} efflux from the endoplasmic reticulum due to the activation of Ryanodine channels blocked Netrin-1-induced axon slowdown. Netrin-1 treatment resulted in a rapid membrane insertion of DCC, followed by a gradual internalization. DCC membrane dynamics were different in the central regions of the growth cones compared to filopodia and axon shafts, highlighting the temporal and spatial heterogeneity in the signaling events downstream of Netrin-1. Cumulatively, these results demonstrate the power of microfluidic compartmentalization and distribution analysis in describing the complex axonal Netrin-1 response.

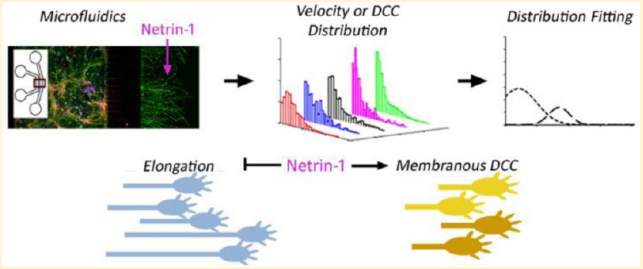

KEYWORDS: *Microfluidics, growth cones, filopodia, receptor dynamics, UNC-5*

A critical aspect of nervous system development and regeneration is the accuracy in the direction and rate of growth of individual axons.[1] The leading tip of an axon is terminated with a growth cone, a highly dynamic, amoeboid structure, sensing and probing the environment for physical and biochemical guidance cues. The growth cone is capable of adjusting the axonal progression according to the guidance cues it encounters on its way. Upon receiving the signal, the growth cone remodels itself by reorganizing its microtubules and actin filaments (F-actin), essential components of the neuronal cytoskeleton.[2] As a result, the axon may be attracted to or repelled form the source of the guidance cue, the growth cone may collapse, or the axon elongation rate may change.[3] Biochemical guidance cues can be either substrate-bound or soluble, affecting the axons either locally or over long distances.[4,5] The major guidance cue families are Slits and Semaphorins (repellent), Ephrins (attractant), and Netrins.[4]

Netrin-1, the best characterized member of the Netrins family, acts not only as a guidance molecule but also as a growth factor. Early studies established Netrin-1 as an attractive guidance cue. However, later studies have shown that, depending on the context, it can also act as a repellent.[6] The origin, age, and developmental stage of neurons have a profound effect on how they respond to Netrin-1.[7] Projecting axons are intended to reach different targets; therefore, even within the same neuronal subtype, growth cones can respond differently to the same guidance cue. This discrepancy has been observed in various in vitro studies.[8−10] Furthermore, the growth cone has to be able to change its responsiveness to Netrin-1, leave the formerly attractive region of its intermediate target, and continue growing toward its ultimate target.[7,11] For example, in the developing rat brain, commissural axons that are attracted by the floor plate cells secreting Netrin-1 lose their responsiveness to Netrin-1 after crossing the midline.[12] The same guidance molecule that initially drew the axon in is now perceived neutral or even as a repellent.[13] This suggests that neurons have a particular flexibility such that they can switch their response to Netrin-1 according to intrinsic or extracellular conditions. Taken together, these studies show that neuronal response to Netrin-1, even within the same neuronal subtype, is inherently heterogeneous. At the molecular level, Netrin-1-induced axon growth depends on many, interdependent factors including the type and density of Netrin-1 receptors,[14] the initial level of the intracellular Ca^{2+} concentration ($[Ca^{2+}]_i$),[15,16]

Received: May 19, 2015
Revised: July 13, 2015
Published: July 20, 2015

DOI: 10.1021/acschemneuro.5b00142
ACS Chem. Neurosci. 2015, 6, 1578−1590

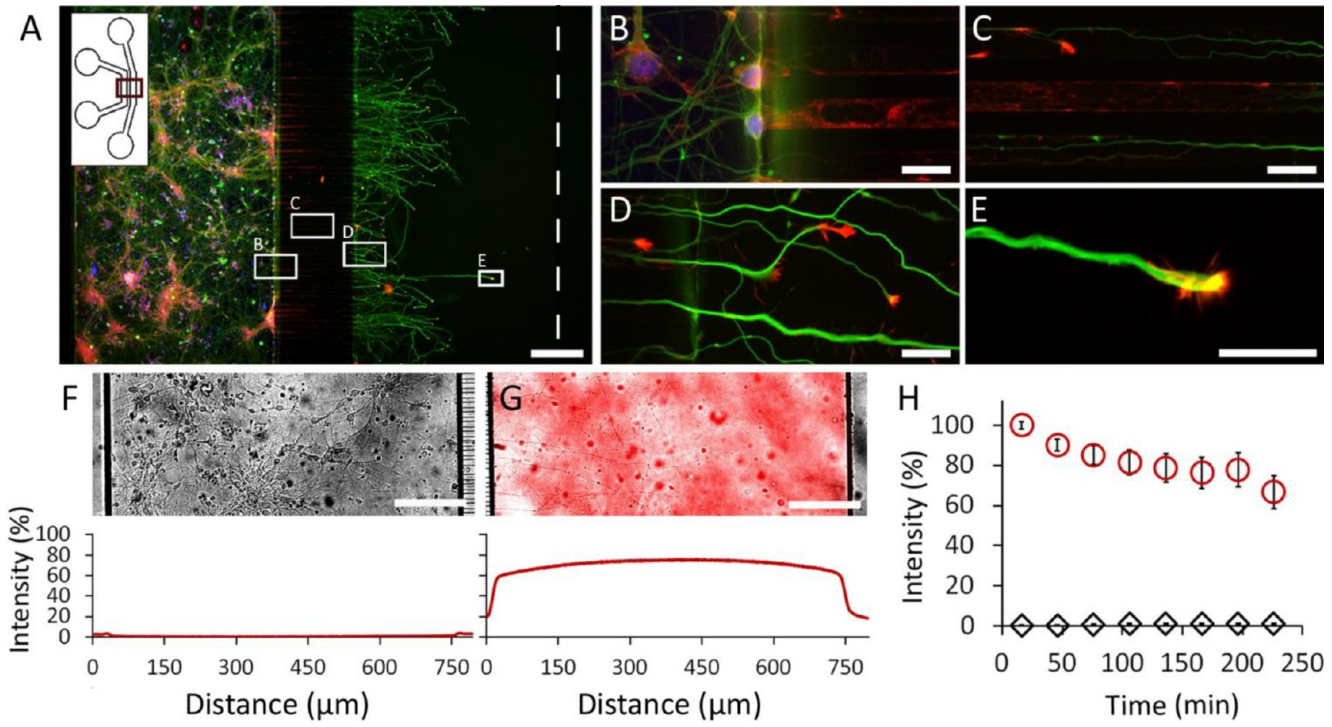

Figure 1. Spatial and fluidic isolation of somata and axons of neurons cultured in the microfluidic devices. (A–E) Mouse cortical neurons at 6 days in vitro with axons extended into axonal compartment of the two compartmental device (inset). Neuronal cytoskeleton was demonstrated by staining βIII-tubulin (green), actin filaments (red), and nuclei (blue). Dashed line indicates the distal end of the axonal compartment. (F, G) 70 kDa RITC-Dextran was used to demonstrate the fluidic isolation between the two compartments. Medium containing the tracer was added to the axonal compartment only, and regular medium with 5 μL volume excess was added to the somatic compartment. Overlays of phase contrast and RITC fluorescence images (top) and normalized intensity plots (bottom) in the somatic (F) and axonal (G) compartments, 4 h after adding the tracer. (H) Fluorescent tracer in axonal (red) and somatic (black) chambers as a function of time. Error bars represent the standard error of the mean for three replicates. Scale bars = 200 μm (A); 20 μm (B–D); 10 μm (E); 100 μm (F, G).

the source and extent of the Ca^{2+} influx,[17] and the ratio of cyclic nucleotides: cyclic adenosine monophosphate (cAMP) and cyclic guanosine monophosphate (cGMP).[15,18]

Netrin-1 interacts with three transmembrane receptor families: Deleted in Colorectal Cancer (DCC),[19] Uncoordinated 5 (UNC-5),[20] and Down Syndrome Cell Adhesion Molecule (DSCAM).[21] However, the presence of additional coreceptors cannot be excluded. Netrin-1 changes the conformations of its receptors, which can then form complexes that induce attraction (DCC/DCC; DSCAM/DSCAM) or repulsion (DSCAM/UNC-5; DCC/UNC-5).[22,23] Downstream of the receptors the information is relayed to Ca^{2+} and cAMP/cGMP second messenger systems.[24] Exposing a growth cone to a concentration gradient of attractive or repulsive guidance cue induces an asymmetric elevation of $[Ca^{2+}]_i$,[11] where the initial level and source of Ca^{2+} regulate the response to Netrin-1.[16,17] The attractive signaling involves activation of two plasma membrane cation channels, transient receptor potential cation channel subfamily C (TRPC) and L-type voltage-dependent Ca^{2+} channel (LVDCC), as well as the release of Ca^{2+} from the endoplasmic reticulum (ER) through ryanodine channels (RyRs).[11] Additionally, if $[Ca^{2+}]_i$ is high enough, RyRs mediate Ca^{2+}-induced Ca^{2+} release (CICR).[25] In the case of Netrin-1-induced repulsion, Ca^{2+} efflux originates from the activation of TRPC1 only; LVDCCs and RyRs are inhibited, and CICR does not take place.[26] The activity of Ca^{2+} channels, in turn, is modulated by cyclic nucleotides. Accordingly, Netrin-1 induces attraction or repulsion through the elevation of cAMP or cGMP levels, respectively.[11,18] Furthermore, second messengers regulate the insertion of receptors to the plasma membrane, which may lead to changes in the axonal response to Netrin-1.[27] Although intensively studied, the complex mechanisms underlying these processes are not fully understood.

Spatial isolation of axons from cell bodies was first achieved by placing a Teflon pad over a scratched tissue culture dish to study the local response of axons to nerve growth factor.[28] A microfluidic device has recently been developed that connects two separate chambers, somatic and axonal, with parallel microchannels that permit the passage of neurites but not somata.[29] A range of microfluidic devices has since been developed for various neurobiological applications.[30] Microfluidic devices facilitate studying neuronal response to guidance cues at single cell or even subcellular levels. This level of detail is typically impeded in the traditional culture systems, where growth cones, axons, and cell bodies not only are in physical contact but also interact with each other chemically. This complex and dynamic microenvironment makes it extremely difficult to elucidate the pathways activated by a particular guidance molecule. Furthermore, culturing neurons in these two-compartmental microfluidic devices allow obtaining a large number of technical replicates, reducing the number of cells required and the experimental workload.

Axon guidance is typically studied by monitoring the turning of individual axons in the presence of a concentration gradient. Traditionally, the gradient has been generated by locally dispensing a concentrated solution using a micropipet.[9,24] The introduction of microfluidic devices enabled the generation of

DOI: 10.1021/acschemneuro.5b00142
ACS Chem. Neurosci. 2015, 6, 1578–1590

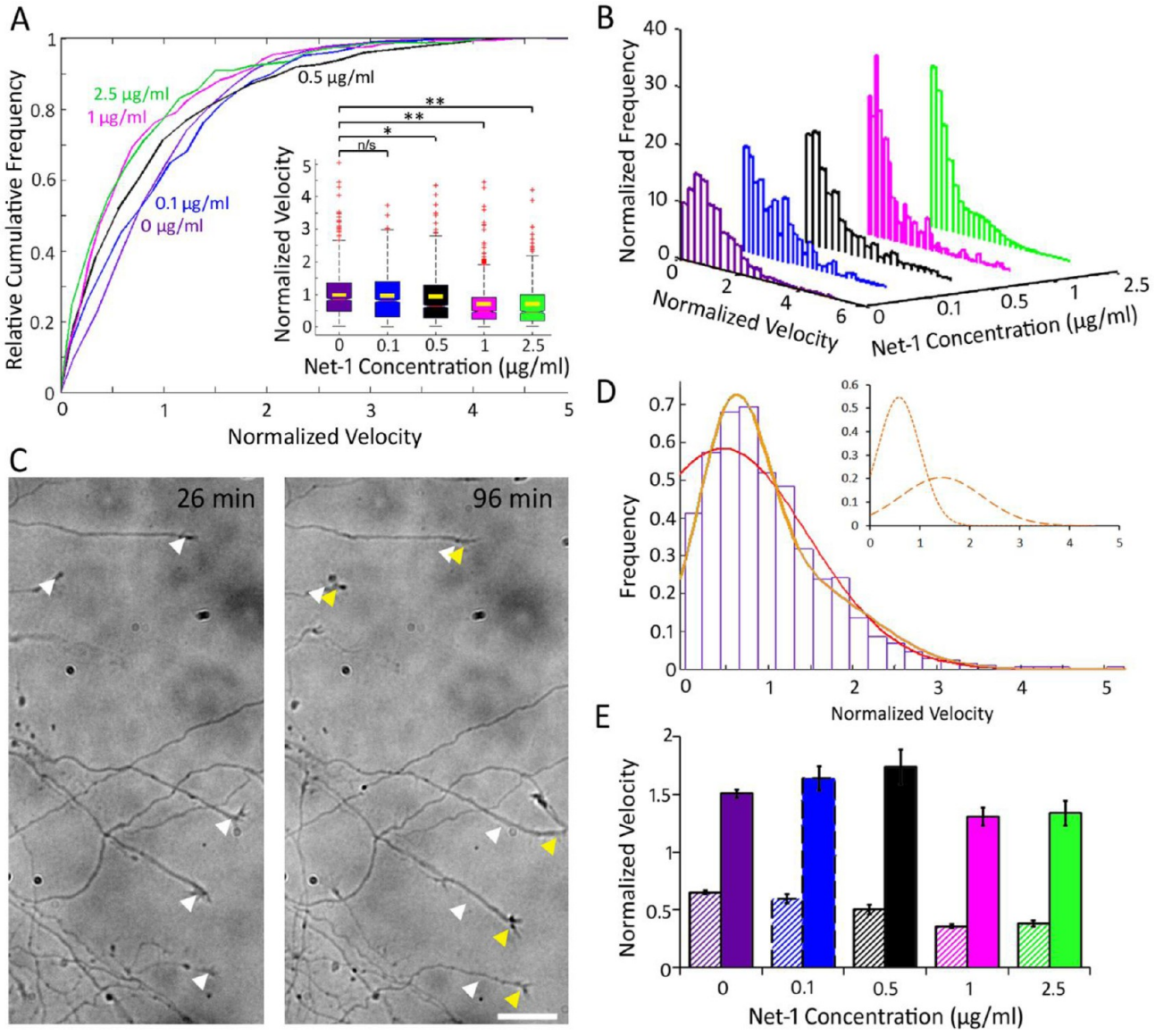

Figure 2. Velocity of cortical axons decreases with increasing concentration of Netrin-1 (Net-1). (A) Relative cumulative frequency plots of normalized axon velocity for varying Netrin-1 concentrations. The inset shows the box plots for increasing concentration of Netrin-1 (Net-1). Red markers show the outliers, and yellow bars show population means. Kruskal–Wallis test ($p < 0.05$) followed by K–S test (*$p < 0.05$, **$p < 0.001$). $N > 100$ axons per condition. (B) Velocity distribution histograms of the same data set. (C) Examples of control axons with similar morphology in the same imaging frame exhibiting different elongation rates as shown by their positions in the initial (left) and final time points (right). White and yellow arrowheads mark initial and final positions of these growth cones, respectively. Scale bar = 10 μm. (D) The control data set was presented as a velocity histogram (purple columns). The same data set was fit with a unimodal truncated Gaussian distribution function (tGDF; red curve) and with a bimodal distribution function (sum of two tGDFs; orange curve). Bimodal distribution provided a better fit as indicated by Akaike and Bayesian model selection criteria. The inset shows the tGDFs for slow (densely dashed line) and fast (sparsely dashed line) subpopulations, which constitute the bimodal distribution. The axis labels are the same as in the histogram. tGDFs for low and fast subpopulations are shown as densely and sparsely dashed lines, respectively. (E) Mean axon velocities of the slow (dashed color) and fast (block color) subpopulations for increasing Netrin-1 concentrations, normalized by the mean velocity of corresponding control group. Note that the presence of two-subpopulations for 0.1 μg/mL treatment was not supported by model selection criteria (dashed column border).

stable gradients, whose profile can be precisely controlled.[31−33] The role of Netrin-1 as a growth factor is rarely the main research objective; it is usually investigated to support turning assay results. Elongation assays measure either the elongation rate or the final length of single axons (dissociated neurons),[9,34,35] or the total or mean length of axon bundles (explants).[21,36,37] Recently, Bhattacharjee et al. performed a more thorough analysis of axonal growth dynamics in response to Netrin-1 concentration gradient, based on a small sample of 11 neurons.[38]

In this paper, we describe the use of a microfluidic device for characterizing the elongation behavior of primary mouse cortical axons in response to isolated Netrin-1 treatment, and the role of Ca^{2+} as a second messenger in Netrin-1 signaling. Moreover, we describe how Netrin-1 affected the localization of its receptor, DCC, on the plasma membrane. Our model system facilitated the treatment and tracking of numerous growth cones simultaneously. Remarkably large numbers of events (>100), obtained for each experimental condition, allowed us to analyze the distribution of axon velocities and

DOI: 10.1021/acschemneuro.5b00142
ACS Chem. Neurosci. 2015, 6, 1578−1590

DCC staining intensities. Based on these parameters, we categorized neurons into two subpopulations which responded differently to Netrin-1.

RESULTS AND DISCUSSION

Isolated Treatment of Axons with Netrin-1 Results in Dose-Dependent Axon Retardation. Neurons survived in the two-compartmental microfluidic devices (Figure 1 and Supporting Information (SI) Figure S1) for at least 11 days in vitro (DIV). Axons, but not somata, crossed through the 300 μm long microchannels, entered the axonal compartment within 3−4 DIV, and reached its half width within 5−6 DIV (Figure 1). This culturing system not only facilitated the spatial isolation of axons and somata but also allowed focusing on a particular developmental age by controlling the length of the microchannels. Furthermore, microfluidics provided the fluidic isolation of the two chambers for at least 4 h, as demonstrated by the exclusion of the fluorescent tracer 70 kDa RITC-Dextran whose molecular weight matches that of Netrin-1 (Figure 1F−H). Creating separate microenvironments for axons and somata provided a better reflection of the in vivo condition, where cell bodies are hundreds of microns away from the tips of elongating axons and are exposed to different concentrations of guidance cues.[39] Additionally, the axonal response to Netrin-1 can be investigated without the contribution of molecules secreted by other cell bodies, i.e., it has been shown that cortical neurons express Netrin-1,[37] and that the basal levels of Netrin-1, as low as 0.5 ng/mL, affect the Netrin-1 sensitivities of axons.[40]

To determine how cortical axons respond to local Netrin-1 treatment, we exposed the axons to varying concentrations of Netrin-1 and measured their elongation rates through time lapse imaging. Velocity vectors of individual axons were determined from the initial and final positions of their growth cones and normalized with the velocities of untreated axons. Our experimental model facilitated the simultaneous stimulation and imaging of over 100 individual axons per circuit, which translates to ca. 1000 axons per imaging session. As a comparison, elongation rates of tens of axons are typically measured in axon turning studies. For example, micropipet experiments permit probing one growth cone at a time, which translates to 10−30 axons per condition.[18,24,35] Furthermore, axon turning experiments usually require the exclusion of slow axons, that is, axons with an elongation rate below an arbitrarily determined cutoff value, which varies from study to study: 5;[22,35,38] 6.7;[24] 7;[9,18] 7.5;[31] and 10 μm/h.[40] Discarding a group of axons with slow elongation rates, especially for elongation rate measurements, does bias the results. The only axon selection criterion in our experimental model was to have passed through the microchannels, that is, being longer than ca. 350 μm at the time of the experiment.

Netrin-1 is commonly associated with an attractive turning response in mammalian cortical neurons, whereas, in our hands Netrin-1 had a suppressing effect and decreased the axon elongation rate (Figure 2A). One possible explanation would be that Netrin-1 regulates the axon elongation rate and turning behavior through different mechanisms.[15,41] Both guidance phenomena, that is, elongation and turning, are required for the correct navigation of axons to their ultimate targets, and act nonexclusively. Immediate, biased turning depends on the molecular gradient experienced by the growth cone; whereas the elongation rate is modulated by the relative concentrations of a guidance molecule over much longer distances, such as the distance between the growth cones and the somata.[41] The latter mode of control is highly relevant to our experimental model where only axons and not cell bodies are stimulated with Netrin-1.

Our axon elongation data is not normally distributed; therefore, we used Kruskal−Wallis test to determine variances and Kolmogorov−Smirnov (K−S) test to compare treatment groups. For the latter, we included Dunn−Sidak p-value correction for multiple comparisons. In our hands, exposure to 0.1 μg/mL Netrin-1 did not result in a significant change in axon elongation ($p < 0.05$; Figure 2A), which is in agreement with earlier studies where low concentrations of Netrin-1 has been shown not to affect axon velocity.[8,33,42] Axons treated with 0.5 μg/mL Netrin-1 had a significantly different velocity distribution compared to control group ($p < 0.05$) and the difference in the velocity distribution became more significant with increasing Netrin-1 concentrations ($p < 0.001$). The velocity distribution in axons treated with 1.0 and 2.5 μg/mL Netrin-1 were similar to each other suggesting that the response reaches its peak around 1.0 μg/mL and remains constant with increasing Netrin-1 concentration. This concentration threshold is on the higher end of spectrum of Netrin-1 concentrations reported in the literature for dissociated mammalian cortical neurons: 0.05 ,[37] 0.25,[23,34] and 1.05 μg/mL.[34] The observation that Netrin-1 affected the velocity distributions, as evidenced by the K−S test results, called for a more detailed distribution analysis.

The Distribution of Axon Velocities Suggests Two Distinct Subpopulations with Different Netrin-1 Sensitivities. High number of observations facilitated by microfluidics translated to over 1000 axons in the control group and a minimum of 100 axons per experimental condition, allowing for a detailed statistical analysis of the axon velocity distribution. Axon velocities normalized with control values were expressed in data histograms (Figure 2B). Heterogeneity in the axon elongation rate was evident in the control group (Figure 2C). We sought to characterize the axon elongation behavior by fitting the velocity data with a unimodal truncated Gaussian distribution function (tGDF) and a bimodal distribution function, which was the sum of two tGDFs. The bimodal distribution provided a better fit to the data, compared to unimodal distribution, as indicated by the corrected Akaike Information Criterion (AIC_c)[43] and Bayesian Information Criterion (BIC).[44] These model selection criteria introduce penalty terms for the number of parameters in each model and thus prevent overfitting. The relative likelihood of the bimodal distribution being a better model than the unimodal distribution was 0.999 and 0.850, in a 0−1 scale, based on bimodal AIC and BIC model weights,[45,46] $w_{bi}(AIC_c)$ and $w_{bi}(BIC)$, respectively, confirming the presence of two neuron subpopulations in the control group (Figure 2D). Therefore, in subsequent analyses, coefficients defining the two tGDFs were used to characterize and compare axon subpopulations. Accordingly, the data for axons treated with varying concentrations of Netrin-1 were fit with unimodal and bimodal distributions. To directly compare the velocity distribution histograms with each other, their frequencies (y-axes) were normalized with those of the control data set such that the total area under each histogram was the same. Two distinct subpopulations were identified for all Netrin-1 concentrations except for 0.1 μg/mL (SI Table S1). The larger (slow) subpopulation, consisting of 57% - 62% of the axons, slowed down in response to 0.5 μg/mL Netrin-1 (22% decrease from

DOI: 10.1021/acschemneuro.5b00142
ACS Chem. Neurosci. 2015, 6, 1578−1590

control velocity). This effect was more pronounced for increasing Netrin-1 concentrations (41% decrease from control velocity for 1.0 μg/mL and above) (Figure 2E). The smaller (fast) subpopulation accelerated by 15% when treated with 0.5 μg/mL Netrin-1 and slowed down by approximately 12% when treated with Netrin-1 at concentrations 1.0 μg/mL and above.

Additionally, our experimental approach allowed for the detection of partial adaptation to Netrin-1. Upon exposure to 1.0 μg/mL Netrin-1, axon velocity initially decreased to 78.4 ± 4.2% of the control velocity, then partially recovered and reached 90.4 ± 4.8% of the control velocity (Figure S2; also see Supplementary Results in the SI). To further determine if the axonal Netrin-1 response was specific to a subpopulation, we imaged a set of axons before and during 1.0 μg/mL Netrin-1 treatment. Consistently, the bimodal model described the data better than unimodal model (Table S2). The slow subpopulation experienced a more pronounced relative slowdown (64%) than the fast subpopulation (35%), indicating that Netrin-1-driven slowdown depends on the initial elongation rate (Figure S3; also see Supplementary Results in the SI). These results cumulatively show that our approach based on velocity distribution analysis was necessary for detecting the two axon subpopulations and the subtle differences in their sensitivity to Netrin-1.

Our finding that two subpopulations exist within primary cortical neurons with different Netrin-1 responses can be interpreted in the light of previous work. Studies on Netrin-1 function typically report two contradictory axon responses within the same population, where one response is dominant. Usually, a group of nonresponsive neurons is also present, further expanding the spectrum. This heterogeneity has been observed in growth cone turning,[22,27] axon branching,[8] as well as in molecular measurements, such as $[Ca^{2+}]_i$.[9] Very recently, cortical neurons have been shown to switch their turning behavior from attraction to repulsion with increasing Netrin-1 concentration.[33] In the nervous system, multiple neuronal subtypes are present within the same anatomical region, which are distinguished based on their phenotypes, morphologies and expression levels of proteins, including ion channels. Furthermore, the attribution of a neuron to a particular subtype can change throughout the development and may be modulated by external stimuli. For example, calcium signaling has been shown to control the differentiation of neurons into different subtypes.[47] These subtypes may have inherent differences in their response to guidance cues. Indeed, the effect of Netrin-1 on neurons has been repeatedly shown to depend on the origin and developmental age of neurons, that is, spatiotemporal dependence.[48,49] This suggests that the axonal response reflects the status of the neuron rather than being an intrinsic property of Netrin-1.[1,50]

The Source of Ca^{2+} Influx and the Basal Cytosolic Ca^{2+} Level Modulate the Axonal Response to Netrin-1. Ca^{2+} plays multiple roles in the functioning of the nervous system and in axon guidance during development. By perturbing various elements of the neuronal Ca^{2+} regulation system we sought to characterize the role of Ca^{2+} in the axonal response to isolated Netrin-1 treatment. We chelated extracellular and intracellular Ca^{2+} by adding EGTA to the treatment medium and by pretreating neurons with BAPTA, respectively. By adding Ryanodine (Ry), we manipulated Ryanodine channels (RyRs) located on the ER membrane, which are known to play a role in the axonal response to Netrin-1.[11] Calcium perturbations induced substantial changes in axon velocities and neuron response to Netrin-1 (Figure 3; Figure S4, Table S3, and also Supplementary Results in the SI). We first

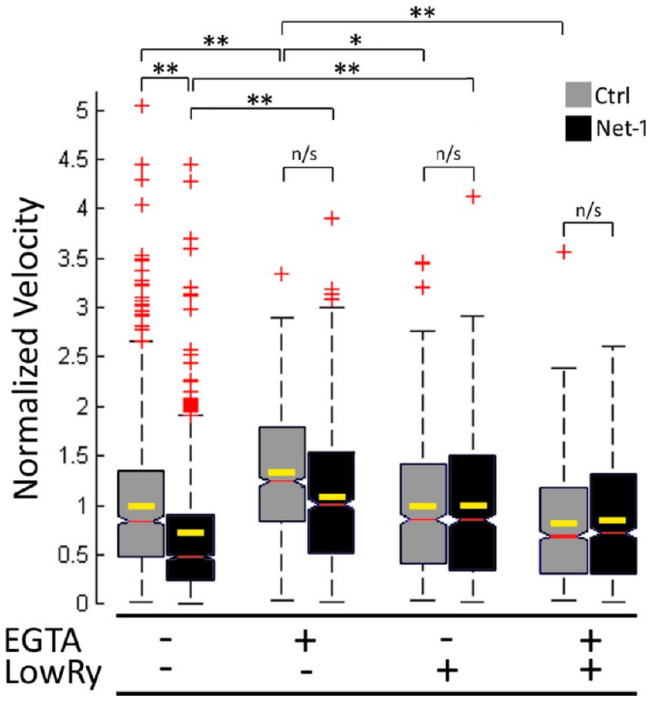

Figure 3. Normalized axon velocity in control (light gray) and Netrin-1 treated (Net-1; dark gray) axons for combinations of EGTA and low Ry. Red markers show the outliers, and red and yellow bars show population medians and means, respectively. Kruskal–Wallis test ($p < 0.05$) followed by K–S test (*$p < 0.05$, **$p < 0.01$). $N > 100$ axons per condition.

investigated the role of Ca^{2+} influx from the extracellular space. Chelating extracellular Ca^{2+} increased the mean velocity of the control axons. This is consistent with earlier reports showing that mammalian cortical neurons accelerate upon inhibition of Ca^{2+} influx through blocking LVDCCs with nifedipine[51] and that *Xenopus* neurons accelerated significantly after reducing extracellular Ca^{2+} concentration from 1.0 mM to 1.0 μM.[35] Axon turning has also been shown to require extracellular Ca^{2+}.[35] Consistently, our results show that axons cotreated with EGTA and 1.0 μg/mL Netrin-1 no longer exhibited a significant slowdown, retaining average velocities at the levels of controls, which was significantly higher than axons treated with Netrin-1 only. These results suggest that axons require the influx of Ca^{2+} from the extracellular space to be able to respond to Netrin-1.

We next investigated the role of Ca^{2+} efflux from the ER in the Netrin-1 response. The mean velocity of control axons did not change when their RyRs were activated with 20 nM Ry (low Ry). However, activation of RyRs, that is, a sustained Ca^{2+} release from the intracellular stores, canceled the observed Netrin-1-induced slowdown (Figure 3). On the other hand, the mean velocity of the control axons decreased by 17.8% (no statistical significance) when RyRs were activated and the extracellular Ca^{2+} was chelated simultaneously. Under these conditions, Netrin-1 did not cause any further reduction in the axon velocity. Activation and inhibition of RyRs have been shown in the literature to accompany Netrin-1 induced attractive and repulsive turning, respectively.[11,18] In our hands, activation of RyRs did not accelerate axons in response

DOI: 10.1021/acschemneuro.5b00142
ACS Chem. Neurosci. 2015, 6, 1578–1590

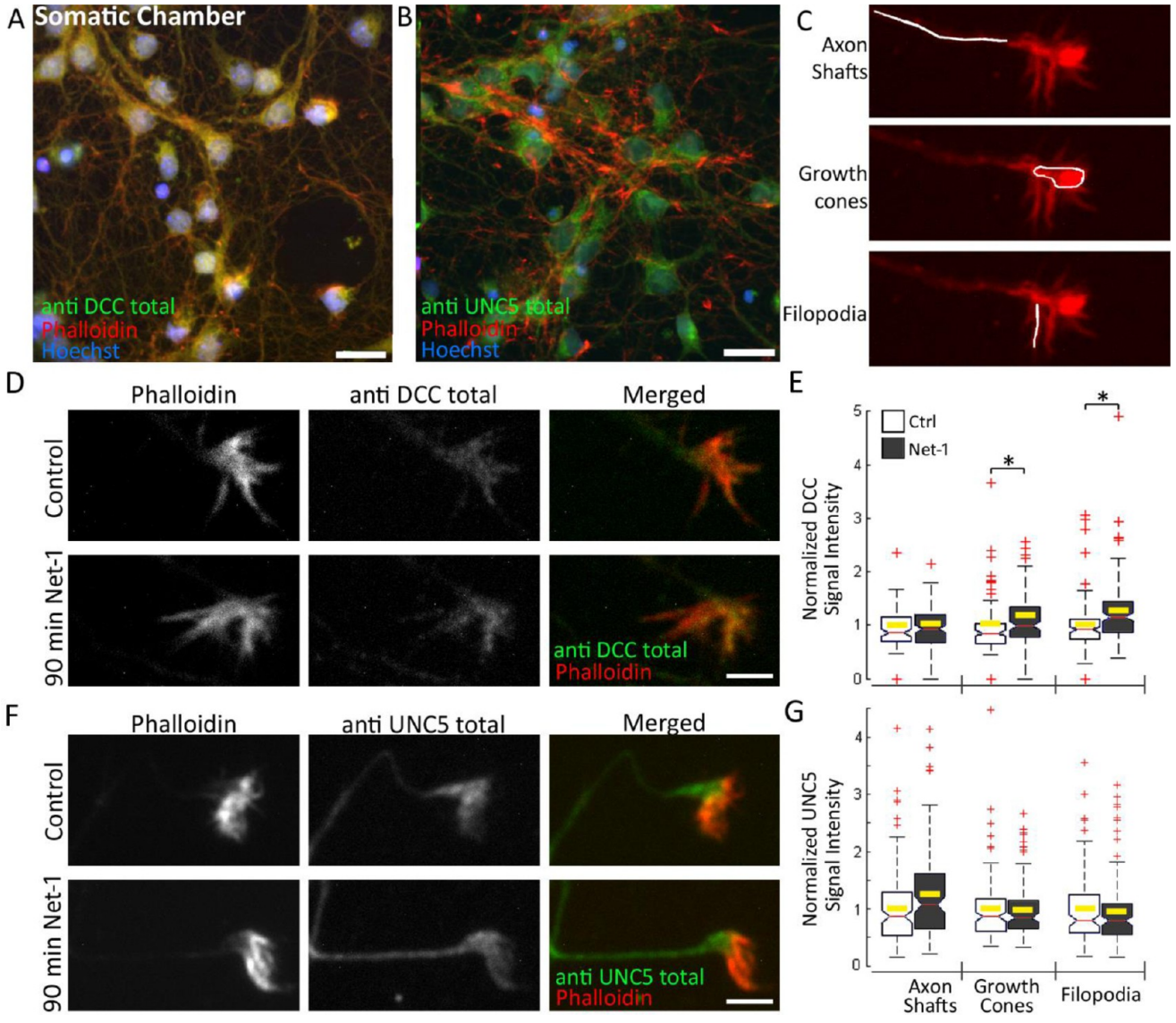

Figure 4. Effect of Netrin-1 (Net-1) treatment on the total level of Netrin-1 receptors. Immunocytochemistry was used to show that DCC (A) and UNC5 (B) were present in the axons and in the cell bodies of control neurons in the somatic chamber. C. Staining intensity was measured in three regions of interest (ROIs): axon shafts, growth cone centers (growth cone), and filopodia. ROIs (white lines and area) were defined in Phalloidin stains. 90 min long axonal treatment with 1.0 μg/mL Netrin-1 induced increases in the total DCC level in growth cones and filopodia (D, E) and in the total UNC5 level in axon shafts (F, G). Background-subtracted DCC (E) and UNC5 (G) signal intensity in three ROIs normalized by the average of the respective control data sets. Red markers show the outliers and yellow bars show population means. Kruskal–Wallis test ($p < 0.05$) followed by K–S test (*$p < 0.05$). Scale bars = 20 μm (A, B); 5 μm (D, F); $N > 100$ axons per condition.

to Netrin-1, but abolished the Netrin-1-induced slowdown. The inhibition of RyRs, however, did not alter the effect of Netrin-1 (Figure S4A, Table S3, and Supplementary Results in the SI). Cumulatively, these results suggest that Netrin-1-induced axon slowdown is mediated by complex $[Ca^{2+}]_i$ dynamics involving Ca^{2+} release from the ER and influx from the extracellular space.

Analyzing axon velocity distributions deemed to be advantageous over comparing mean axon velocities: treatments that did not affect mean axon velocities appeared to have pronounced effects on velocity distributions, as shown in velocity histograms (Figure S4 and S5) and according to the K–S test (Table S3 and Supplementary Results in the SI). However, there was not sufficient statistical evidence to identify neuron subpopulations in the Ca^{2+} perturbation data sets (Table S4 and Supplementary Results in the SI).

Netrin-1 Treatment Modulates the Total Available Pools of Its Receptors DCC and UNC5. To determine the relative changes in the total and membranous UNC5 and DCC receptor levels upon Netrin-1 stimulation, we conducted immunocytochemistry. Membrane permeabilization enabled the quantification of the total levels of receptors, whereas using an antibody that targets the extracellular epitope of the DCC without permeabilizing the membrane enabled the quantification of DCC present on the plasma membrane. Both UNC5 and DCC were detected in the entire neuron, including the cell body (Figure 4A and B); consistent with earlier work using cortical neurons.[36,37,52,53] The presence of receptors in all subcellular regions is in agreement with the notion that neurons may be sensing differences in Netrin-1 concentration along their entire lengths to modulate their elongation rates, and across their growth cones to modulate

DOI: 10.1021/acschemneuro.5b00142
ACS Chem. Neurosci. 2015, 6, 1578–1590

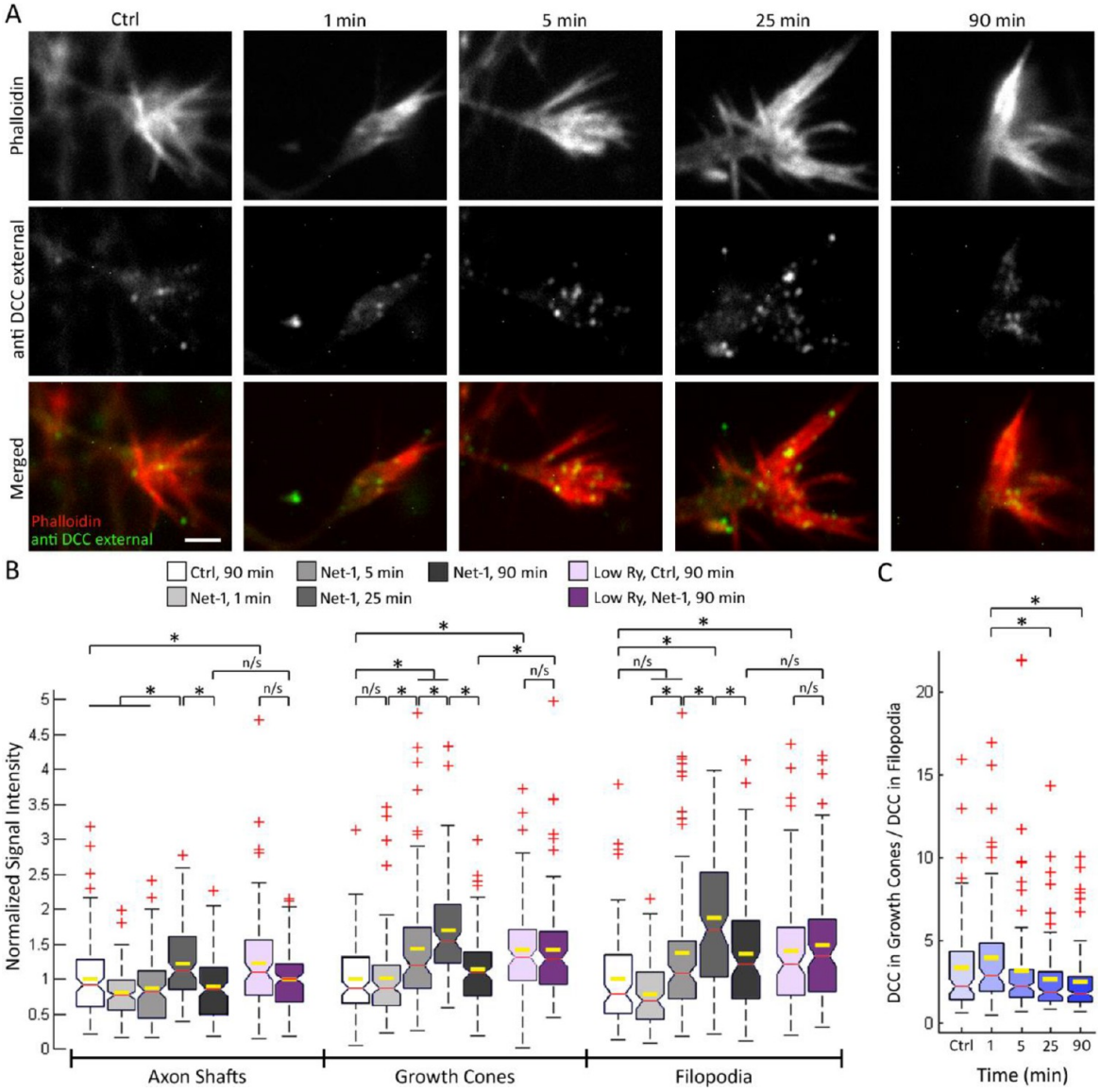

Figure 5. Effect of Netrin-1 (Net-1) treatment and Ryanodine activation on the distribution of Netrin-1 receptors. (A) Axonal treatment with 1.0 μg/mL Netrin-1 induced time-dependent increases in the DCC presence on cell membranes. Scale bar = 3 μm. (B) Background-subtracted average signal intensity in three ROIs normalized by the average of the respective control data set. Activation of the ryanodine receptors with low Ry was sufficient to insert DCC to the membranes of growth cones and filopodia. (C) Ratio of normalized membranous DCC signal in filopodia and corresponding growth cones during Netrin-1 treatment. Red markers show the outliers, and yellow bars show population means. Kruskal–Wallis test ($p < 0.05$), followed by K–S test (*$p < 0.05$). $N > 100$ axons per condition.

turning responses. Signal intensities were measured at three axonal regions of interest (ROIs): axon shafts, growth cones, and filopodia (Figure 4C), for over 1000 neurons. Results from separate experiments showed that at 90 min time point, Netrin-1 increased the total levels of DCC by 1.2× and 1.3× in growth cones and filopodia, respectively, but it did not affect the DCC levels in axon shafts (Figure 4D and E). In contrast, Netrin-1 induced a 1.2× increase in the total UNC5 levels in the axon shaft (no statistical significance), but it did not affect the UNC5 levels in the growth cones or in filopodia (Figure 4F and G). Our results show that Netrin-1 affects the size of the available receptor pools, and that these changes depend highly on the subcellular region, such as axon shafts or filopodia. While the underlying causes of this heterogeneous response remain elusive, these results suggest that axonal guidance mechanisms downstream of Netrin-1 stimulation involves the spatiotemporal dynamics of Netrin-1 receptors.

Netrin-1 and Ryanodine Regulate the Membrane Presence of DCC. Dynamic changes in the levels of membranous DCC were investigated by incubating axons with 1.0 μg/mL Netrin-1 for different time periods: 1, 5, 25, and 90 min. The control group underwent a 90 min-long incubation with medium lacking Netrin-1. In the growth cones, Netrin-1 induced a rapid insertion of DCC to the membranes, consistent with the previous reports,[36] where the background-subtracted DCC staining intensity rose to 1.4× of its initial value after 5 min of treatment. At 25 min, the signal reached 1.7× and then gradually decreased, eventually reaching 1.3× at 90 min time point. In the filopodia, membranous DCC signal intensity initially decreased (0.8× of the control value at 1 min) before rising to 1.4× at 5 min and reaching a peak of 1.9× at 25

DOI: 10.1021/acschemneuro.5b00142
ACS Chem. Neurosci. 2015, 6, 1578–1590

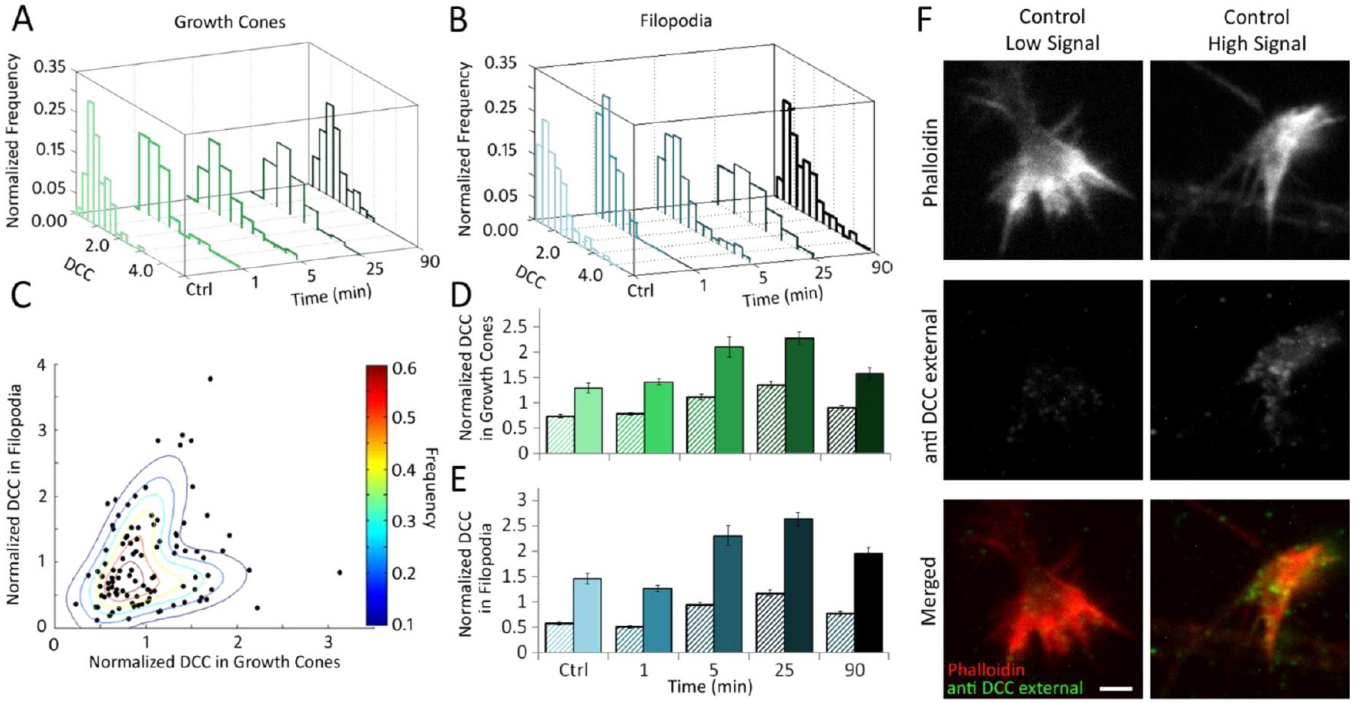

Figure 6. Distribution of membranous DCC indicates the presence of two subpopulations with different temporal dynamics in different subcellular regions. DCC staining intensity in growth cones (A) and filopodia (B) is expressed as data histograms for each time point following 1.0 μg/mL Netrin-1 treatment. N = 521 axons for all time points. The bimodal distribution (sum of two GDFs) provided a better fit than the unimodal distribution (single GDF) as suggested by model selection criteria. (C) Bimodal distribution was used to fit normalized DCC signal intensity in filopodia vs growth cones of the same axons. Average staining intensities were obtained for each subpopulation for growth cones (D), and for filopodia (E) using the fit functions suggested by the bimodal distribution model. (F) Examples of untreated (control) growth cones with high and low DCC signal. Scale bar = 3 μm.

min. At 90 min, the signal intensity in filopodia was 1.4× of its initial value. In the axon shafts, the initial decrease of membranous DCC signal lasted longer. The signal decreased to 0.8× at 1 min, partially recovered (0.9×) at 5 min, and surpassed the initial value (1.2×) at 25 min time point. At 90 min, DCC intensity in the axon shafts was 0.9× of its initial value (Figure 5A and B). These results show that Netrin-1 affects the membrane presence of DCC in a dynamic fashion. A rapid and subtle decrease (axon shafts and filopodia only) may be accounted for a localized adaptation response.[54] The subsequent pronounced increase shared by all three ROIs is in agreement with the notion that Netrin-1 recruits DCC and stabilizes it on the membrane.[36] The internalization of the DCC-Netrin-1 complex was initially suppressed, but eventually recovered, resulting in a progressive decrease in the membranous DCC. Our data show that the temporal dynamics of DCC recruitment upon Netrin-1 treatment correlate with the partial recovery of the axon elongation rate during Netrin-1 treatment (Figure S2 and see Supplementary Results in the SI). Membranous DCC levels have been shown to affect the sensitivity of neurons to Netrin-1,[53,54] where a high DCC level has been linked to enhanced axon outgrowth from explants in response to Netrin-1.[37] Our experiments performed with older neurons suggest an opposite mechanism: the membrane insertion of DCC intensified the neuron retardation, and the subsequent internalization of DCC resulted in a recovery of the axon velocity. Interestingly, DCC has recently been shown to be involved in axon slowdown due to another guidance molecule, Draxin.[55] DCC may be involved in the regulation of the magnitude but not the character, that is, acceleration or slowdown, of the Netrin-1 response.

We next determined if Netrin-1-induced insertion of DCC into growth cones and filopodia membranes was regulated by intracellular Ca^{2+} dynamics, similar to the effects of Netrin-1 on axon elongation. Neurons treated with low Ry to induce sustained Ca^{2+} efflux from the ER exhibited an increase in the membranous DCC staining at 90 min time point in growth cones and filopodia. The increase in the membranous DCC in growth cones induced by low Ry exceeded the increase induced by Netrin-1. When low Ry-treated axons were cotreated with Netrin-1, no further increase in the membranous DCC was observed in growth cones and in filopodia. These findings show that both intracellular Ca^{2+} release and Netrin-1 stimulation are sufficient to induce DCC membrane insertion; however, it is not clear whether Netrin-1 regulates DCC insertion directly or through inducing Ca^{2+} release via RyRs. Furthermore, although the activation of RyRs induced DCC membrane insertion, it did not affect axon elongation rate. This suggests that the secondary mechanisms downstream of DCC, Ca^{2+} efflux from ER stores in particular, cannot accelerate or decelerate axons directly, but may be regulating the magnitude of Netrin-1-induced axon acceleration or deceleration through modulating the membrane presence of Netrin-1 receptors.

The temporal dynamics of the membranous DCC staining revealed regional differences: in growth cones DCC increase was evident as early as 5 min into Netrin-1 treatment, whereas in axon shafts and filopodia the increase was observed at 25 min time point. These subcellular differences were also evident when non-normalized growth cone:filopodium signal ratios in individual axons were considered (Figure 5C; SI Figure S7 and Table S7). At 1 min after Netrin-1 treatment, this ratio was 1.2× higher than the control value (no statistical significance)

DOI: 10.1021/acschemneuro.5b00142
ACS Chem. Neurosci. 2015, 6, 1578−1590

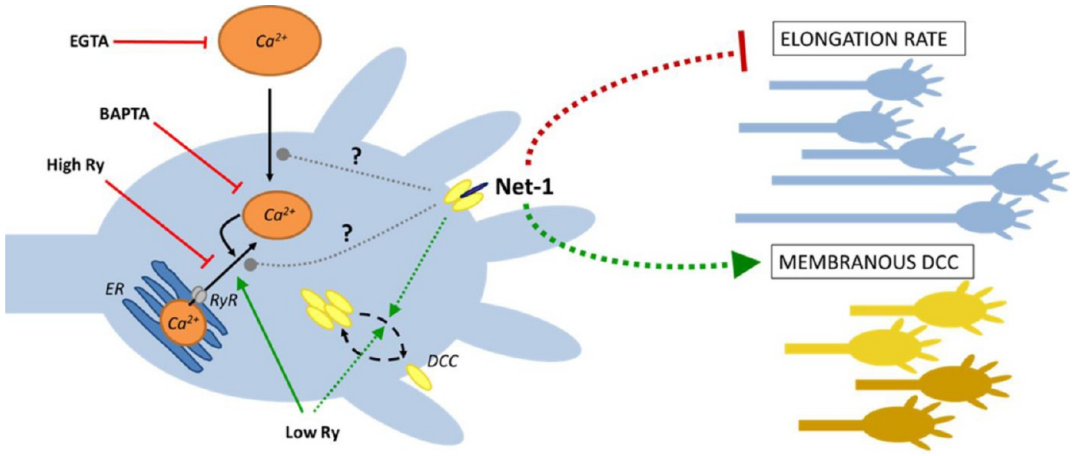

Figure 7. Putative mechanisms for axonal response to uniform concentration of Netrin-1 (Net-1) and its regulation by Ca^{2+} signaling. In axons, intracellular Ca^{2+} concentration ($[Ca^{2+}]_i$) is tightly regulated despite high concentrations in the extracellular space and in internal stores, primarily the endoplasmic reticulum (ER). Netrin-1 induces Ca^{2+} efflux to the cytosol. Basal level of $[Ca^{2+}]_I$ and the Ca^{2+} influxes modulate axonal response to Netrin-1. Extracellular and intracellular Ca^{2+} is chelated with EGTA and BAPTA, respectively. Efflux from the ER is modulated by either inhibiting or activating the Ryanodine channel (RyR) with high or low concentrations of Ryanodine (Ry), respectively. Two neuron subpopulations were identified based on their elongation behavior in control conditions. The relative sizes of slow and fast subpopulations are represented by short and long axons, respectively. Although the Ca^{2+} dependency is too complex to depict here, the overall effect of Netrin-1 is a reduction in the average axon elongation rate, which is more pronounced in the slow subpopulation. Netrin-1 receptor DCC cycles between the cytosolic pool and the plasma membrane. Two axon subpopulations were identified based on the staining intensity of the membranous DCC in control conditions. The relative sizes of subpopulations with high and low DCC are represented by their shade of yellow. Both Netrin-1 and Low Ry treatments stimulated the recruitment of DCC to the plasma membrane, yet with different dynamics in the high and low DCC subpopulations. Dotted lines represent indirect effects.

and logarithmically decreased to 0.7× of the control value at 90 min. These results suggest that Netrin-1 induces a spatially coordinated DCC trafficking response in growth cone membranes.

This subcellular, regional heterogeneity in axonal response to Netrin-1 is consistent with a previous report. In *Xenopus* neurons, Netrin-1 gradient has been shown to induce different signaling mechanisms in growth cone centers and in filopodia.[24] According to a model proposed by Nicol and colleagues,[24] Netrin-1 induces a short-term elevation in cAMP levels in filopodia, which causes a brief increase in the frequency of Ca^{2+} transients. In contrast, in the growth cone center, Netrin-1 induces a sustained increase in the frequency of Ca^{2+} transients, which causes a transient increase in the cAMP levels. Interestingly, both events have been shown to depend on the availability of DCC receptors.[24] While Ca^{2+} transients and cAMP dynamics are outside the scope of this paper, taking into account that Ca^{2+} and cAMP modulate membrane trafficking of Netrin-1 receptors,[14] we speculate that the differential effects of Netrin-1 on DCC membrane trafficking in different growth cone regions may be due to the differences in second messenger dynamics.

Furthermore, artificial elevation of cAMP level in different growth cone compartments had different effects on axon elongation and did not diminish the variation in the axon velocities within the same neuron population.[24] Our data, together with these observations, suggest that highly compartmentalized and dynamic changes in receptor membrane presence and second messenger activity may be regulating the axon elongation behavior, for example, in response to guidance cues. Further experiments are required to identify the causal relation between receptor membrane cycling, localized second messenger activity and neuron growth behavior.

Distribution Analysis Suggests Two Distinct Subpopulations with Different Spatiotemporal DCC Dynamics and Netrin-1 Sensitivities. To gain more insight into DCC temporal dynamics, the data sets were subjected to distribution analysis. We assessed if there were neuron subpopulations that exhibit different DCC membrane recruitment dynamics in response to Netrin-1treatment (Figure 6). Histograms were generated for each time point and for each subcellular region (Figure 6A and B, SI Figure S6) and model selection criteria (Table S5) were used to determine the better fit between the unimodal (single GDF) and bimodal (a sum of two GDFs) Gaussian mixture models. In untreated controls, two distinct subpopulations were detected based on DCC immunostaining. 46.7% and 47.4% of axons with lower DCC staining in the central parts of the growth cones and in filopodia, respectively, were assigned to subpopulation 1. Axons with higher staining were assigned to subpopulation 2. Fitting normalized DCC signal intensities in filopodia and growth cones belonging to the same axon with a two-dimensional bimodal Gaussian distribution (Figure 6C; SI Table S7) confirmed the size fraction of low DCC subpopulation as 47%. In growth cones, the subpopulations differed only by their initial DCC levels and exhibited the same response to Netrin-1 (Figure 6D). In filopodia, the subpopulations differed in their DCC membrane insertion and subsequent internalization dynamics. Subpopulation 2 exhibited a more pronounced increase in the membranous DCC signal in response to Netrin-1 (Figure 6E).

We next investigated if there was a correlation between the membranous DCC staining and the axon elongation rate, by fixing and staining neurons at the end of an elongation experiment under control conditions. The microfluidic device greatly facilitated the matching of individual axons in the live-cell experiments with those in immunofluorescence images. No correlation was detected when axon velocities and growth cone

DOI: 10.1021/acschemneuro.5b00142
ACS Chem. Neurosci. 2015, 6, 1578−1590

DCC staining intensities were plotted against each other for individual axons (Figure S8) in control conditions, suggesting that the subpopulations based on axon velocity and based on membranous DCC are not related despite their similar size.

SUMMARY AND CONCLUSIONS

Netrin-1 is a bifunctional neuronal guidance cue and growth factor that plays an important role during embryonic development and during the regeneration of adult neurons. Research has been focused on the molecular mechanisms that regulate growth cone turning toward Netrin-1; however, the role of Netrin-1 in regulating the elongation rate of axons is not well understood. By exploiting the microfluidic isolation of axons from their somata, we characterized the elongation behavior and receptor membrane trafficking in a large number of axons that were locally exposed to Netrin-1 and treated with drugs that modulate intracellular Ca^{2+} dynamics. Changes in the axon elongation behavior in a neuron subpopulation were only detected through distribution analysis, which requires a large sample size. We show that the Netrin-1-induced axon slowdown is mediated by complex Ca^{2+} dynamics and involves Ca^{2+} efflux from the ER via the Ryanodine channels. In parallel, we describe the dynamics of DCC, a Netrin-1 receptor, which was rapidly employed to cell membranes upon Netrin-1 stimulation. Interestingly, DCC membrane presence was also increased when the Ryanodine channels were activated pharmacologically, suggesting that second messengers are orchestrating the Netrin-1 response in developing axons (Figure 7). Furthermore, Netrin-1 affects DCC dynamics differently at different subcellular locations, such as the central regions of the growth cones and filopodia, which is in agreement with other studies describing the spatiotemporal dynamics of second messenger activity. Taken together, these results link Netrin-1 and its receptors to second messengers; however, further studies are needed to fully characterize how axon elongation is orchestrated upon Netrin-1 stimulation. Among many open questions in Netrin-1 signaling, two, in particular, may benefit from microfluidic neuron culture: (i) Are there different mechanisms in the axonal response to Netrin-1 concentration gradients vs uniform Netrin-1 concentrations? (ii) Does soma-axon communication coordinate axonal Netrin-1 response? The former question can be addressed with different microfluidic designs involving concentration gradients that are parallel[56] or orthogonal[33] to the direction of initial axonal growth. The latter question can be addressed by using the circuit design presented in this study by treating fluidically isolated somata and subsequently observing axon behavior.

METHODS

Microfluidic Cell Culture and Treatments. Masters of two-compartmental microfluidic devices were fabricated through photolithography as previously described.[56] Polydimethylosiloxane (PDMS) pads were replica molded and bonded to glass coverslips using O_2 plasma. Devices were UV sterilized, coated with poly-L-lysine overnight and rinsed with phosphate buffered saline (PBS). Mouse cortical neurons were obtained from embryonic day 14 CD-1 outbred mouse and dissociated according to established protocols.[56] Neurons were seeded in the somatic chamber at a density of approximately 8×10^5 cells/cm^2 and maintained in a tissue culture incubator (5% CO_2, 37 °C) in DMEM-Glutamax medium containing 10% fetal bovine serum, Pen/Strep, and B_{27} neuron supplement (all from Gibco, Dun Laoghaire, Ireland). At 3 DIV, the medium was replaced with Neurobasal medium (Gibco) containing Pen/Strep and B_{27}. See Supporting Methods in the SI for details. Experiments were conducted at 5−7 DIV after the growth cones have reached the middle of the axonal chamber. Axons were treated with Netrin-1 (R&D Systems, Abingdon, U.K.). Extracellular Ca^{2+} was chelated with 2 mM ethylene glycoltetraacetic acid (EGTA; Sigma, Wicklow, Ireland). Ca^{2+} release from the internal stores was induced with 20 nM ryanodine (Ry; Calbiochem, Carrigtwohill, Ireland). Ry treatment included a 40 min long incubation prior the experiment.

Live Cell imaging. Live cell imaging was performed at 5−6 DIV. Media in both compartments were replaced with Neurobasal medium with Pen/Strep and B_{27}, buffered with 25 mM HEPES (Sigma) and containing Netrin-1 or vehicle (H_2O). Isolated treatment of axons with Netrin-1 was achieved by adding 5 μL less medium to the axonal compartment compared to the somatic compartment. Up to nine circuits were placed in a Petri dish 10 cm in diameter. The coverslips were stabilized on the Petri dish using Tack-it adhesive. A 1 mL solution of 0.1% ethylenediaminetetraacetic acid (EDTA, Sigma) in DI water was added to the Petri dish to minimize evaporation of the medium during live imaging. Five to six positions were chosen to image as many single, nonoverlapping growth cones as possible. Axons were imaged from 25 ± 5 min to 95 ± 5 min following the treatment. The long experiment consisted of 1.5 h long imaging of neurons in the control conditions, replacement of medium in the wells either with the treatment medium or with control medium and 1.5 h long second imaging period. The analysis of axon velocity in the second imaging period was based on the images obtained from 110 to 180 min. The Petri dish containing the devices was placed under an inverted microscope equipped with a motorized stage (Zeiss, Cambridge, U.K.), an EMCCD camera (Hamamatsu, Hertfordshire, U.K.) and an environmental chamber (Life Imaging Services, Basel, Switzerland), which maintained the temperature at 37 °C. Phase contrast images were taken every 10 min with a 40× 0.6 NA objective.

Quantification of Axon Elongation and Distribution Analysis. Axon elongation was analyzed in terms of velocity vector, that is, the position vector between the initial and final positions of the growth cone divided by time. The data for each condition was collected from at least five independent experiments, for which the cells were obtained from at least two separate dissections. NIH ImageJ software (National Institutes of Health, Bethesda, MD) and MtrackJ plug-in was used to track the movement of growth cones.[57] The velocities of individual axons were normalized with the average axon velocity in the control cultures from the same dissection. Normalized velocity values of individual axons in control cultures were presented in a velocity histogram. The optimal bin size for the histogram was determined by using a cost function following the method by Shimazaki and Shinomoto.[58] The optimal bin size was different for each data set, altering the area under the histograms. To be able to directly compare the histograms obtained from different data sets with each other, the frequency values were multiplied with a bin size correction factor such that the areas under the histograms were equal to that of the control data set. This bin size correction factor was defined as the bin size of the control data set divided by the bin size of the treatment data set. The data sets were fit with a unimodal truncated Gaussian distribution function or a bimodal truncated Gaussian distribution function using distribution fitting application in Matlab (MathWorks, Natick, MA) with custom defined distribution functions (see the SI for the equations). Additionally, we imposed an overlap constraint for the fits with bimodal distribution such that the overlap between the two components was less than 50% of either component. The size fraction of the slow subpopulation in the control and 1.0 μg/mL Netrin-1 treatment data sets (0.58 and 0.61, respectively) was used as a guideline for fitting the remaining Netrin-1 data sets. The size fractions for the 0.1, 0.5, and 2.5 μg/mL data sets were therefore constrained in the 0.57−0.62 range. This alteration did not significantly affect the likelihood of the fit or the model selection criteria. Likelihood values returned by the distribution fitting application were used to calculate Akaike Information Criterion (AIC_c)[43] and Bayesian Information Criterion (BIC).[44] The relative likelihood of the bimodal or the unimodal distribution being a better model was expressed in a 0−1 scale using AIC_c and BIC model weights,[45,46] $w(AIC_c)$ and w(BIC),

DOI: 10.1021/acschemneuro.5b00142
ACS Chem. Neurosci. 2015, 6, 1578−1590

respectively (see the SI for the definitions of these metrics). The value 0.85 was considered to be a sufficient weight to reject the alternative model. Once the fit parameters were determined, Matlab-generated sets of random numbers were generated to calculate mean velocities and standard deviations for each subpopulation. The data sets were generated such that the number of positive events was equal to 10 000. Only positive values were used to find the mean velocity of the subpopulation. The large number of events minimized the variation due to random number generation (SEM < 0.5% for 5 sets of random numbers). The SEM values of the subpopulation velocities were calculated from the obtained standard deviation and the estimated number of axons for each subpopulation (number of axons multiplied by the size fraction). For the experiment where the velocities of individual axons were compared before and after Netrin-1 treatment, the data was fit with the two-dimensional unimodal Gaussian distribution and the two-dimensional bimodal Gaussian mixture distribution, that is, nontruncated forms, and the Akaike- and Bayes-derived criteria were calculated accordingly.

Immunocytochemistry. Cells were fixed on 5−7 DIV through incubation with 0.5% glutaraldehyde (Sigma) for 15 min at room temperature (RT) and subsequent rinsing with PBS. Immunocytochemistry in the microfluidic devices followed similar protocols as for the cultures on glass slides.[59] The solutions were introduced to only one well of each compartment, which guaranteed pressure-driven flow through the compartments. Cells were treated for 30 min with a blocking buffer composed of 1% bovine serum albumin (BSA; Sigma) in PBS. To determine cytosolic levels of DCC and UNC5 and to stain tubulin cells were treated with the blocking buffer containing 0.5% Triton X-100 (Sigma). Blocking buffer without Triton X-100 was used to study DCC presence on the cell membrane. Cells were incubated with 1:100 mouse anti-DCC (Calbiochem), 1:100 rabbit anti-UNC5H2 (Santa Cruz Biotechnology, Heidelberg, Germany), or 1:300 mouse anti-βIII-tubulin (Promega, Kilkenny, Ireland) antibodies diluted in blocking buffer for 1 h at RT. Subsequently, cells were washed twice with PBS and incubated with the following secondary antibodies diluted in blocking buffer for 1 h at RT: Alexa488 goat anti-mouse (1:300; Invitrogen); Alexa555 goat anti-rabbit (1:100; Invitrogen). To stain F-actin, cells were treated with Alexa568 Phalloidin (1:200; Invitrogen) or Alexa488 Phalloidin (1:150; Invitrogen). Finally, cells were washed with PBS, counterstained with Hoechst (33342, Invitrogen) for 15 min at RT, washed with PBS and DI water, and mounted in Moviol (Sigma). For the experiment investigating the correlation between axon elongation rate and membranous DCC staining, the neurons were fixed immediately after periodic imaging of elongating axons.

Quantification of Receptor Levels and Distribution Analysis. To quantify the change in receptor levels upon Netrin-1 treatment, control and experimental cultures were prepared under identical conditions in separate circuits bonded on the same coverslip. Imaging was performed using an inverted, epifluorescent microscope (Olympus, Southend-on-Sea, U.K.) equipped with a CCD camera (Hamamatsu). Somatic and axonal compartments were imaged in DAPI, FITC, and TRITC channels. ROIs were selected based on Phalloidin staining. Approximately 100 ROIs were selected from three independent cell cultures for each condition. Mean pixel intensity for each ROI was measured in each channel using ImageJ software. Background signal intensity defined as the intensity of the cell-free area neighboring the ROI was subtracted from the signal intensity of ROI in both channels. The signal intensity of the receptor in the cytosolic pool (acquired through membrane permeabilization) was normalized with the Phalloidin signal intensity obtained from the same ROI, The staining intensity of the membranous receptor was normalized only with the membranous receptor signal intensity of the control group. Statistical analysis of membranous DCC signal intensity distribution was similar to the analysis of the velocity distribution. Staining intensity histograms were plotted and the data sets were fit with unimodal Gaussian distribution and bimodal Gaussian mixture distribution models. Model selection criteria were used to pick the best fitting model. Similar to elongation data, a maximum of 50% overlap between the two components were considered in fitting bimodal distributions. The size fractions of the low DCC subpopulation in the control group based on growth cone and filopodia signals (0.467 and 0.474, respectively) were used as a guideline for fitting the remaining data sets. The size fraction was constrained in a range of 0.42−0.52. Mean signal intensities, standard deviations and SEM values for each subpopulation were calculated from the fit parameters.

Statistical Analysis. The data for each condition was tested for normality using Lilliefors test. If one or more data sets was not normally distributed, the nonparametric Kruskal−Wallis test was used for variance analysis, followed by Kolmogorov−Smirnov test for comparing individual treatment groups. For the latter one, Dunn-Sidak p-value correction was used to account for multiple comparisons. Significance level was 0.05, unless stated otherwise. In box-and-whisker plots, the central indent and the red mark represents median, the edges of the box present the 25th (q1) and 75th (q3) percentiles, respectively. The whiskers extend to the most extreme data points not considered outliers. Outliers are defined as numbers greater than q3 + 1.5(q3−q1) or less than q1−1.5(q3−q1).

■ ASSOCIATED CONTENT

Supporting Information

Supplementary Results and Discussion; Supplementary Methods; six tables; eight figures; equations for unimodal and bimodal distribution models and for calculating statistical model criteria. The Supporting Information is available free of charge on the ACS Publications website at DOI: 10.1021/acschemneuro.5b00142.

■ AUTHOR INFORMATION

Corresponding Authors

*E-mail: gil.lee@ucd.ie.

*E-mail: devrim.kilinc@ucd.ie

Author Contributions

†G.U.L. and D.K. share the last authorship of this paper. All authors designed the experiments. A.B. conducted the experiments. A.B. and D.K. analyzed the results. All authors wrote the paper.

Funding

This material is based upon works supported by Science Foundation Ireland (SFI) under Grant No. 08/RP1/81376 and 08/IN1/82072 (G.U.L.) and the Nanoremedies Programme funded under the Programme for Research in Third-Level Institutions and cofunded under the European Regional Development Fund (G.U.L.). A.B. is a recipient of AXA Doctoral Fellowship, and D.K. is a recipient of Marie Curie Intra-European Fellowship.

Notes

The authors declare no competing financial interest.

■ ACKNOWLEDGMENTS

We thank D. Gandhi and A. Pandya for their assistance in generating three-dimensional charts and contour plots in Matlab. We thank S. Andraszewicz at the Swiss Federal Institute of Technology Zurich for her suggestions in statistical methods. We thank A. Lesniak for her help in harvesting neurons.

■ REFERENCES

(1) Song, H., and Poo, M. (2001) The cell biology of neuronal navigation. *Nat. Cell Biol. 3*, E81−8.

(2) Kalil, K., and Dent, E. W. (2005) Touch and go: guidance cues signal to the growth cone cytoskeleton. *Curr. Opin. Neurobiol. 15*, 521−6.

DOI: 10.1021/acschemneuro.5b00142
ACS Chem. Neurosci. 2015, 6, 1578−1590

(3) Bashaw, G. J., and Klein, R. (2010) Signaling from axon guidance receptors. *Cold Spring Harbor Perspect. Biol. 2*, a001941.
(4) Huber, A. B., Kolodkin, A. L., Ginty, D. D., and Cloutier, J. F. (2003) Signaling at the growth cone: ligand-receptor complexes and the control of axon growth and guidance. *Annu. Rev. Neurosci. 26*, 509−63.
(5) Geraldo, S., and Gordon-Weeks, P. R. (2009) Cytoskeletal dynamics in growth-cone steering. *J. Cell Sci. 122*, 3595−604.
(6) Chisholm, A., and Tessier-Lavigne, M. (1999) Conservation and divergence of axon guidance mechanisms. *Curr. Opin. Neurobiol. 9*, 603−15.
(7) Shewan, D., Dwivedy, A., Anderson, R., and Holt, C. E. (2002) Age-related changes underlie switch in netrin-1 responsiveness as growth cones advance along visual pathway. *Nat. Neurosci. 5*, 955−62.
(8) Dent, E. W., Barnes, A. M., Tang, F., and Kalil, K. (2004) Netrin-1 and semaphorin 3A promote or inhibit cortical axon branching, respectively, by reorganization of the cytoskeleton. *J. Neurosci. 24*, 3002−12.
(9) Hong, K., Nishiyama, M., Henley, J., Tessier-Lavigne, M., and Poo, M. (2000) Calcium signalling in the guidance of nerve growth by netrin-1. *Nature 403*, 93−8.
(10) Kothapalli, C. R., van Veen, E., de Valence, S., Chung, S., Zervantonakis, I. K., Gertler, F. B., and Kamm, R. D. (2011) A high-throughput microfluidic assay to study neurite response to growth factor gradients. *Lab Chip 11*, 497−507.
(11) Tojima, T., Hines, J. H., Henley, J. R., and Kamiguchi, H. (2011) Second messengers and membrane trafficking direct and organize growth cone steering. *Nat. Rev. Neurosci. 12*, 191−203.
(12) Shirasaki, R., Katsumata, R., and Murakami, F. (1998) Change in chemoattractant responsiveness of developing axons at an intermediate target. *Science 279*, 105−7.
(13) Dickson, B. J. (2002) Molecular mechanisms of axon guidance. *Science 298*, 1959−64.
(14) Round, J., and Stein, E. (2007) Netrin signaling leading to directed growth cone steering. *Curr. Opin. Neurobiol. 17*, 15−21.
(15) Forbes, E. M., Thompson, A. W., Yuan, J., and Goodhill, G. J. (2012) Calcium and cAMP levels interact to determine attraction versus repulsion in axon guidance. *Neuron 74*, 490−503.
(16) Zheng, J. Q. (2000) Turning of nerve growth cones induced by localized increases in intracellular calcium ions. *Nature 403*, 89−93.
(17) Ooashi, N., Futatsugi, A., Yoshihara, F., Mikoshiba, K., and Kamiguchi, H. (2005) Cell adhesion molecules regulate Ca2+-mediated steering of growth cones via cyclic AMP and ryanodine receptor type 3. *J. Cell Biol. 170*, 1159−67.
(18) Nishiyama, M., Hoshino, A., Tsai, L., Henley, J. R., Goshima, Y., Tessier-Lavigne, M., Poo, M. M., and Hong, K. (2003) Cyclic AMP/GMP-dependent modulation of Ca2+ channels sets the polarity of nerve growth-cone turning. *Nature 423*, 990−5.
(19) Keino-Masu, K., Masu, M., Hinck, L., Leonardo, E. D., Chan, S. S., Culotti, J. G., and Tessier-Lavigne, M. (1996) Deleted in Colorectal Cancer (DCC) encodes a netrin receptor. *Cell 87*, 175−85.
(20) Leonardo, E. D., Hinck, L., Masu, M., Keino-Masu, K., Ackerman, S. L., and Tessier-Lavigne, M. (1997) Vertebrate homologues of C. elegans UNC-5 are candidate netrin receptors. *Nature 386*, 833−8.
(21) Ly, A., Nikolaev, A., Suresh, G., Zheng, Y., Tessier-Lavigne, M., and Stein, E. (2008) DSCAM is a netrin receptor that collaborates with DCC in mediating turning responses to netrin-1. *Cell 133*, 1241−54.
(22) Hong, K., Hinck, L., Nishiyama, M., Poo, M. M., Tessier-Lavigne, M., and Stein, E. (1999) A ligand-gated association between cytoplasmic domains of UNC5 and DCC family receptors converts netrin-induced growth cone attraction to repulsion. *Cell 97*, 927−41.
(23) Purohit, A. A., Li, W., Qu, C., Dwyer, T., Shao, Q., Guan, K. L., and Liu, G. (2012) Down syndrome cell adhesion molecule (DSCAM) associates with uncoordinated-5C (UNC5C) in netrin-1-mediated growth cone collapse. *J. Biol. Chem. 287*, 27126−38.
(24) Nicol, X., Hong, K. P., and Spitzer, N. C. (2011) Spatial and temporal second messenger codes for growth cone turning. *Proc. Natl. Acad. Sci. U. S. A. 108*, 13776−81.
(25) Fill, M., and Copello, J. A. (2002) Ryanodine receptor calcium release channels. *Physiol. Rev. 82*, 893−922.
(26) Tojima, T. (2012) Intracellular signaling and membrane trafficking control bidirectional growth cone guidance. *Neurosci. Res. 73*, 269−74.
(27) Bartoe, J. L., McKenna, W. L., Quan, T. K., Stafford, B. K., Moore, J. A., Xia, J., Takamiya, K., Huganir, R. L., and Hinck, L. (2006) Protein interacting with C-kinase 1/protein kinase Calpha-mediated endocytosis converts netrin-1-mediated repulsion to attraction. *J. Neurosci. 26*, 3192−205.
(28) Campenot, R. B. (1977) Local control of neurite development by nerve growth factor. *Proc. Natl. Acad. Sci. U. S. A. 74*, 4516−9.
(29) Taylor, A. M., Rhee, S. W., Tu, C. H., Cribbs, D. H., Cotman, C. W., and Jeon, N. L. (2003) Microfluidic Multicompartment Device for Neuroscience Research. *Langmuir 19*, 1551−1556.
(30) Taylor, A. M., and Jeon, N. L. (2010) Micro-scale and microfluidic devices for neurobiology. *Curr. Opin. Neurobiol. 20*, 640−7.
(31) Morel, M., Shynkar, V., Galas, J. C., Dupin, I., Bouzigues, C., Studer, V., and Dahan, M. (2012) Amplification and temporal filtering during gradient sensing by nerve growth cones probed with a microfluidic assay. *Biophys. J. 103*, 1648−56.
(32) Xiao, R. R., Zeng, W. J., Li, Y. T., Zou, W., Wang, L., Pei, X. F., Xie, M., and Huang, W. H. (2013) Simultaneous generation of gradients with gradually changed slope in a microfluidic device for quantifying axon response. *Anal. Chem. 85*, 7842−50.
(33) Taylor, A. M., Menon, S., and Gupton, S. L. (2015) Passive microfluidic chamber for long-term imaging of axon guidance in response to soluble gradients. *Lab Chip 15*, 2781−9.
(34) Zhu, K., Chen, X., Liu, J., Ye, H., Zhu, L., and Wu, J. Y. (2013) AMPK interacts with DSCAM and plays an important role in netrin-1 induced neurite outgrowth. *Protein Cell 4*, 155−61.
(35) Ming, G. L., Song, H. J., Berninger, B., Holt, C. E., Tessier-Lavigne, M., and Poo, M. M. (1997) cAMP-dependent growth cone guidance by netrin-1. *Neuron 19*, 1225−35.
(36) Bouchard, J. F., Moore, S. W., Tritsch, N. X., Roux, P. P., Shekarabi, M., Barker, P. A., and Kennedy, T. E. (2004) Protein kinase A activation promotes plasma membrane insertion of DCC from an intracellular pool: A novel mechanism regulating commissural axon extension. *J. Neurosci. 24*, 3040−50.
(37) Bouchard, J. F., Horn, K. E., Stroh, T., and Kennedy, T. E. (2008) Depolarization recruits DCC to the plasma membrane of embryonic cortical neurons and enhances axon extension in response to netrin-1. *J. Neurochem. 107*, 398−417.
(38) Bhattacharjee, N., Li, N., Keenan, T. M., and Folch, A. (2010) A neuron-benign microfluidic gradient generator for studying the response of mammalian neurons towards axon guidance factors. *Integr Biol. (Camb). 2*, 669−79.
(39) Dickson, B. J., and Zou, Y. (2010) Navigating intermediate targets: the nervous system midline. *Cold Spring Harbor Perspect. Biol. 2*, a002055.
(40) Ming, G. L., Wong, S. T., Henley, J., Yuan, X. B., Song, H. J., Spitzer, N. C., and Poo, M. M. (2002) Adaptation in the chemotactic guidance of nerve growth cones. *Nature 417*, 411−8.
(41) Mortimer, D., Pujic, Z., Vaughan, T., Thompson, A. W., Feldner, J., Vetter, I., and Goodhill, G. J. (2010) Axon guidance by growth-rate modulation. *Proc. Natl. Acad. Sci. U. S. A. 107*, 5202−7.
(42) Winkle, C. C., McClain, L. M., Valtschanoff, J. G., Park, C. S., Maglione, C., and Gupton, S. L. (2014) A novel Netrin-1-sensitive mechanism promotes local SNARE-mediated exocytosis during axon branching. *J. Cell Biol. 205*, 217−32.
(43) Hurvich, C. M., and Tsai, C. L. (1995) Model Selection for Extended Quasi-Likelihood Models in Small Samples. *Biometrics 51*, 1077−1084.
(44) Kass, R. E., and Raftery, A. E. (1995) Bayes Factors. *J. Am. Stat. Assoc. 90*, 773−795.

DOI: 10.1021/acschemneuro.5b00142
ACS Chem. Neurosci. 2015, 6, 1578−1590

(45) Burnham, K. P., and Anderson, D. R. (2001) Kullback-Leibler information as a basis for strong inference in ecological studies. *Wildl. Res. 28*, 111−119.
(46) Buckland, S. T., Burnham, K. P., and Augustin, N. H. (1997) Model selection: An integral part of inference. *Biometrics 53*, 603−618.
(47) Rosenberg, S. S., and Spitzer, N. C. (2011) Calcium signaling in neuronal development. *Cold Spring Harbor Perspect. Biol. 3*, a004259.
(48) Bradford, D., Cole, S. J., and Cooper, H. M. (2009) Netrin-1: diversity in development. *Int. J. Biochem. Cell Biol. 41*, 487−93.
(49) Fothergill, T., Donahoo, A. L., Douglass, A., Zalucki, O., Yuan, J., Shu, T., Goodhill, G. J., and Richards, L. J. (2014) Netrin-DCC signaling regulates corpus callosum formation through attraction of pioneering axons and by modulating Slit2-mediated repulsion. *Cereb Cortex. 24*, 1138−51.
(50) Dent, E. W., Tang, F., and Kalil, K. (2003) Axon guidance by growth cones and branches: common cytoskeletal and signaling mechanisms. *Neuroscientist 9*, 343−53.
(51) Hutchins, B. I., and Kalil, K. (2008) Differential outgrowth of axons and their branches is regulated by localized calcium transients. *J. Neurosci. 28*, 143−53.
(52) Goldman, J. S., Ashour, M. A., Magdesian, M. H., Tritsch, N. X., Harris, S. N., Christofi, N., Chemali, R., Stern, Y. E., Thompson-Steckel, G., Gris, P., Glasgow, S. D., Grutter, P., Bouchard, J. F., Ruthazer, E. S., Stellwagen, D., and Kennedy, T. E. (2013) Netrin-1 promotes excitatory synaptogenesis between cortical neurons by initiating synapse assembly. *J. Neurosci. 33*, 17278−89.
(53) Moore, S. W., Correia, J. P., Lai Wing Sun, K., Pool, M., Fournier, A. E., and Kennedy, T. E. (2008) Rho inhibition recruits DCC to the neuronal plasma membrane and enhances axon chemoattraction to netrin 1. *Development 135*, 2855−64.
(54) Moore, S. W., and Kennedy, T. E. (2006) Protein kinase A regulates the sensitivity of spinal commissural axon turning to netrin-1 but does not switch between chemoattraction and chemorepulsion. *J. Neurosci. 26*, 2419−23.
(55) Ahmed, G., Shinmyo, Y., Ohta, K., Islam, S. M., Hossain, M., Naser, I. B., Riyadh, M. A., Su, Y., Zhang, S., Tessier-Lavigne, M., and Tanaka, H. (2011) Draxin inhibits axonal outgrowth through the netrin receptor DCC. *J. Neurosci. 31*, 14018−23.
(56) Kilinc, D., Blasiak, A., O'Mahony, J. J., and Lee, G. U. (2014) Low piconewton towing of CNS axons against diffusing and surface-bound repellents requires the inhibition of motor protein-associated pathways. *Sci. Rep. 4*, 7128.
(57) Meijering, E., Dzyubachyk, O., and Smal, I. (2012) Methods for Cell and Particle Tracking. In *Imaging and Spectroscopic Analysis of Living Cells: Optical and Spectroscopic Techniques* (Conn, P. M., Ed.), pp 183−200, Elsevier Academic Press, San Diego.
(58) Shimazaki, H., and Shinomoto, S. (2007) A method for selecting the bin size of a time histogram. *Neural Comput. 19*, 1503−27.
(59) Glynn, M. W., and McAllister, A. K. (2006) Immunocytochemistry and quantification of protein colocalization in cultured neurons. *Nat. Protoc. 1*, 1287−96.

DOI: 10.1021/acschemneuro.5b00142
ACS Chem. Neurosci. 2015, 6, 1578−1590